Available online at www.sciencedirect.com
ScienceDirect
Journal of Sound and Vibration 319 (2009) 1–14
JOURNAL OF SOUND AND VIBRATION
www.elsevier.com/locate/jsvi

Rapid Communication

Multiple internal resonances and non-planar dynamics of shallow suspended cables to the harmonic excitations

Lianhua Wang*, Yueyu Zhao

College of Civil Engineering, Hunan University, Changsha, Hunan 410082, PR China

Received 17 April 2008; received in revised form 7 August 2008; accepted 20 August 2008
Handling Editor: L.G. Tham
Available online 2 October 2008

Abstract

In the present study, the nonlinear response of a shallow suspended cable with multiple internal resonances to the primary resonance excitation is investigated. The method of multiple scales is applied directly to the nonlinear equations of motion and associated boundary conditions to obtain the modulation equations and approximate solutions of the cable. Frequency–response curves and force–response curves are used to study the equilibrium solution and its stability. The effects of the excitation amplitude on the frequency–response curves of the cable are also analyzed. Moreover, the chaotic dynamics of the shallow suspended cable is investigated by means of numerical simulations.

1. Introduction

Cable structures, which have importance in many engineering applications such as voltage transmission lines, stay cables and mooring cables, have been investigated for a long time. Many studies have been performed on large amplitude vibrations of cable structures, and many different methods to investigate the nonlinear dynamics have been applied. An interesting literature review of work on the nonlinear dynamics of cables to the harmonic excitations can be found in the related papers by Rega [1].

In distributed-parameter systems, the nonlinearities of the structure may activate nonlinear modal interaction due to the presence of internal resonances among different modes [2]. Depending on the values of the elasto-geometric parameter, different internal resonances may be activated. In the past decades, there has been considerable interest in the study of nonlinear dynamics of cable structures to the harmonic excitations with one-to-one internal resonances [3,4], two-to-one internal resonances [5–10] and multiple internal resonances [11–14]. As a result of these internal resonances, cables may exhibit very rich complex nonlinear dynamics. Moreover, long cables inherent to low damping may be prone to large amplitude vibration. Therefore, many studies have investigated the vibration mitigation of the cables [15–18]. However, some nonlinear interaction phenomena due to the internal resonances may be observed in controlled cables [17,18].

*Corresponding author. Tel.: +86 731 8823962; fax: +86 731 8822029.
E-mail address: lhwang@hnu.cn (L. Wang).

0022-460X/$ - see front matter © 2008 Elsevier Ltd. All rights reserved.
doi:10.1016/j.jsv.2008.08.020

Recently, many studies have been performed on the nonlinear interaction and large amplitude vibration of a suspended cable with a three-to-one internal resonance. Lacarbonara and Rega [19] have shown that three-to-one internal resonances might be activated between the symmetric in-plane modes. Applying different methods, the present authors [20–22] investigated the nonlinear response of the suspended cable with the three-to-one internal resonance. Moreover, numerical simulations were used to illustrate the chaotic dynamics of the cable. However, these studies focused only on the in-plane nonlinear response of the cable. Therefore, some inherent prosperities such as the overall flexibility are ignored. In fact, the one-to-one internal resonances between in-plane and out-of-plane modes are always presented for the shallow suspended cable [19]. Therefore, the non-planar response of the cable is desired in order to capture the more accurate dynamic characteristics and reflect the overall flexibility.

In this paper we extend our previous work [20,21] to consider the out-of-plane motion of a shallow suspended cable. The three-to-one internal resonance between the third and the first symmetric in-plane modes ($\omega_3^{\text{in}} \approx 3\omega_1^{\text{in}}$) and the one-to-one internal resonance between the third symmetric in-plane mode and the third symmetric out-of-plane mode ($\omega_3^{\text{in}} \approx \omega_3^{\text{out}}$) are taken into account. The case of the primary resonance of the first symmetric mode ($\Omega \approx \omega_1^{\text{in}}$) is also considered. The method of multiple scales is applied to obtain the second-order uniform asymptotic solutions of the cable. Moreover, the equilibrium solutions and dynamic solutions of the modulation equations are investigated.

2. Equations of motions

In this study, our attention is focused on a shallow suspended cable with span l and sag b. A Cartesian coordinate system $Oxyz$ is chosen, with the origin O placed at the left support of the cable. The static and dynamic configurations of the cable are shown in Fig. 1. Neglecting the bending, torsional and shear rigidities, and assuming that the suspended cable stretches in a *quasi-static* manner [6], the non-dimensional equation governing the in-plane and out-of-plane motion of the cable can be written as [12,23]

$$\ddot{v} + 2c_v\dot{v} - v'' - \alpha(v'' + y'')\int_0^1 \left\{ y'v' + \frac{1}{2}(v'^2 + w'^2) \right\} \mathrm{d}x = F(x)\cos(\Omega t), \tag{1}$$

$$\ddot{w} + 2c_w\dot{w} - w'' - \alpha w''\int_0^1 \left\{ y'v' + \frac{1}{2}(v'^2 + w'^2) \right\} \mathrm{d}x = 0, \tag{2}$$

where $y(x) = 4fx(1-x)$ is the initial parabolic shape of the cable; $f = b/l$ is the sag-to-span ratio; $\alpha = EA/H = 8bEA/(mgl^2)$ is the non-dimensional stiffness parameter [19]; m the mass per unit length; E the Young modulus; A the area of the cross section; g the gravitational acceleration; c_v and c_w are the non-dimensional viscous damping coefficients; v and w denote the non-dimensional in-plane and out-of-plane displacements, respectively; the overdot and prime indicate the derivatives with respect to the non-dimensional time t and coordinate x; and $F(x)$ and Ω are the spatial distribution and the non-dimensional frequency of the harmonic excitation, respectively. Moreover, the boundary conditions are given by

$$v(x,t) = w(x,t) = 0 \quad \text{at } x = 0 \text{ and } x = 1. \tag{3}$$

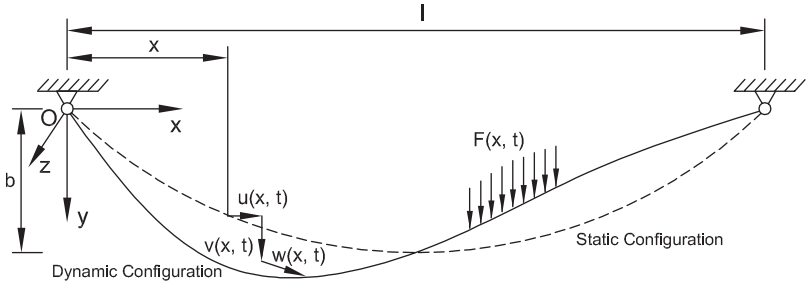

Fig. 1. The static and dynamic configurations of a shallow suspended cable.

3. Perturbation analysis

In this study, the method of multiple scales [24] is applied directly to determine the second-order uniform expansion of the nonlinear response of the cables. Following the standard details of the multiple scales method, we introduce the new independent time variables:

$$T_i = \varepsilon^i t \quad (i = 0, 1, 2, \ldots), \tag{4}$$

where ε is a small non-dimensional bookkeeping parameter. Then, we have the differential operators

$$\frac{\mathrm{d}}{\mathrm{d}t} = D_0 + \varepsilon D_1 + \varepsilon^2 D_2 + \cdots, \quad \frac{\mathrm{d}^2}{\mathrm{d}t^2} = D_0^2 + 2\varepsilon D_0 D_1 + \varepsilon^2 (D_1^2 + 2D_0 D_2) + \cdots, \tag{5}$$

where $D_n = \partial/\partial T_n$. Moreover, in order to balance the nonlinearities, damping and resonances, we rescale the c_v, c_w and F as $\varepsilon^2 c_v$, $\varepsilon^2 c_w$ and $\varepsilon^2 F$. Because the resonant terms appear at the third order, we can seek uniform expansions of non-dimensional displacements in the following forms:

$$v(x,t) = \sum_{i=1}^{3} \varepsilon^i v_i(x, T_0, T_2) + \cdots, \tag{6}$$

$$w(x,t) = \sum_{i=1}^{3} \varepsilon^i w_i(x, T_0, T_2) + \cdots. \tag{7}$$

Substituting Eqs. (6) and (7) into Eqs. (1) and (2) and equating the coefficients of like power of ε on the left-side and the right- side of the equation, the following differential equations can be obtained.

Order ε:

$$D_0^2 v_1 - v_1'' - \alpha y'' \int_0^1 v_1' y' \,\mathrm{d}x = 0, \tag{8}$$

$$D_0^2 w_1 - w_1'' = 0. \tag{9}$$

Order ε^2:

$$D_0^2 v_2 - v_2'' - \alpha y'' \int_0^1 v_2' y' \,\mathrm{d}x = \alpha v_1'' \int_0^1 y' v_1' \,\mathrm{d}x + \frac{1}{2}\alpha y'' \int_0^1 (v_1' v_1' + w_1' w_1') \,\mathrm{d}x, \tag{10}$$

$$D_0^2 w_2 - w_2'' = \alpha w_1'' \int_0^1 y' v_1' \,\mathrm{d}x. \tag{11}$$

Order ε^3:

$$\begin{aligned} D_0^2 v_3 - v_3'' - \alpha y'' \int_0^1 v_3' y' \,\mathrm{d}x = & -D_0 D_2 v_1 - 2c_v D_0 v_1 + \alpha v_1'' \int_0^1 y' v_2' \,\mathrm{d}x + \alpha v_2'' \int_0^1 y' v_1' \mathrm{d}x \\ & + \alpha y'' \int_0^1 (v_1' v_2' + w_1' w_2') \,\mathrm{d}x + \frac{1}{2}\alpha v_1'' \int_0^1 (v_1' v_1' + w_1' w_1') \,\mathrm{d}x + F \cos \Omega T_0, \end{aligned} \tag{12}$$

$$D_0^2 w_3 - w_3'' = -D_0 D_2 w_1 - 2c_w D_0 w_1 + \alpha w_1'' \int_0^1 y' v_2' \,\mathrm{d}x + \alpha w_2'' \int_0^1 y' v_1' \,\mathrm{d}x + \frac{1}{2}\alpha w_1'' \int_0^1 (v_1' v_1' + w_1' w_1') \,\mathrm{d}x, \tag{13}$$

where $D_i = \partial/\partial T_i$. The boundary conditions are given by

$$v_i(x, T_0, T_2) = 0, \quad w_i(x, T_0, T_2) = 0 \ \text{ at } x = 0 \text{ and } x = 1 \text{ for } i = 1, 2, 3. \tag{14}$$

Because all the modes that are not directly or indirectly excited will die out after a long time due to the damping effect [24], the first and third symmetric in-plane modes and the out-of-plane solution are assumed to

include in the first-order solution in order to account for the three-to-one and one-to-one internal resonances:

$$v_1 = A_1(T_2)\phi_1(x)e^{i\omega_1^{in}T_0} + A_3(T_2)\phi_3(x)e^{i\omega_3^{in}T_0} + cc, \tag{15}$$

$$w_1 = B_3(T_2)\varphi_3(x)e^{i\omega_3^{out}T_0} + cc, \tag{16}$$

where $\phi_i(x)$ and ω_i^{in} are the ith symmetric in-plane mode and the corresponding frequency, $\varphi_3(x)$ and ω_3^{out} are the third symmetric out-of-plane mode and the corresponding frequency (see Appendix A), cc stands for the complex conjugate of the preceding terms, and $A_1(T_2)$, $A_3(T_2)$ and $B_3(T_2)$ are the complex-valued functions of T_2. Substituting Eqs. (15) and (16) into Eqs. (10) and (11), we can obtain

$$\begin{aligned} D_0^2 v_2 - v_2'' - \alpha y'' \int_0^1 v_2' y' \,dx = {} & \Pi_1 A_1^2 e^{2i\omega_1^{in}T_0} + \Pi_2 A_3^2 e^{2i\omega_3^{in}T_0} + \Pi_3 A_1 A_3 e^{i(\omega_3^{in}+\omega_1^{in})T_0} \\ & + \Pi_4 A_3 \bar{A}_1 e^{i(\omega_3^{in}-\omega_1^{in})T_0} + \Pi_5 A_1 \bar{A}_1 + \Pi_6 A_3 \bar{A}_3 + \Pi_7 B_3^2 e^{2i\omega_3^{out}T_0} + \Pi_8 B_3 \bar{B}_3 + cc, \end{aligned} \tag{17}$$

$$\begin{aligned} D_0^2 w_2 - w_2'' = {} & \Pi_9 A_1 B_3 e^{i(\omega_1^{in}+\omega_3^{out})T_0} + \Pi_{10} A_3 B_3 e^{i(\omega_3^{in}+\omega_3^{out})T_0} + \Pi_{11} B_3 \bar{A}_1 e^{i(\omega_3^{out}-\omega_1^{in})T_0} \\ & + \Pi_{12} B_3 \bar{A}_3 e^{i(\omega_3^{out}-\omega_3^{in})T_0} + cc, \end{aligned} \tag{18}$$

where Π_i $(i = 1, \ldots, 6)$ are defined in Ref. [20], and

$$\Pi_7 = \Pi_8 = \frac{1}{2}\alpha y'' \int_0^1 \varphi_3' \varphi_3' \,dx, \quad \Pi_9 = \Pi_{10} = \alpha \varphi_3'' \int_0^1 y_1' \phi_1' \,dx, \quad \Pi_{11} = \Pi_{12} = \alpha \varphi_3'' \int_0^1 y_1' \phi_3' \,dx. \tag{19}$$

Then the solutions of Eqs. (17) and (18) can be written as follows:

$$\begin{aligned} v_2 = {} & A_1^2 e^{2i\omega_1^{in}T_0} \Psi_1(x) + A_3^2 e^{2i\omega_3^{in}T_0} \Psi_2(x) + A_3 A_1 e^{i(\omega_1^{in}+\omega_3^{in})T_0} \Psi_3(x) + A_3 \bar{A}_1 e^{i(\omega_3^{in}-\omega_1^{in})T_0} \Psi_4(x) \\ & + A_1 \bar{A}_1 \Psi_5(x) + A_3 \bar{A}_3 \Psi_6(x) + B_3^2 e^{2i\omega_3^{out}T_0} \Psi_7(x) + B_3 \bar{B}_3 \Psi_8(x) + cc, \end{aligned} \tag{20}$$

$$\begin{aligned} w_2 = {} & A_1 B_3 e^{i(\omega_1^{in}+\omega_3^{out})T_0} \Psi_9(x) + A_3 B_3 e^{i(\omega_3^{in}+\omega_3^{out})T_0} \Psi_{10}(x) + B_3 \bar{A}_1 e^{i(\omega_3^{out}-\omega_1^{in})T_0} \Psi_{11}(x) \\ & + B_3 \bar{A}_3 e^{i(\omega_3^{out}-\omega_3^{in})T_0} \Psi_{12}(x) + cc, \end{aligned} \tag{21}$$

where the second-order shape functions $\Psi_i(x)$ $(i = 1, \ldots, 12)$ are the solutions of the following boundary-value problem:

$$\Psi_1'' + \alpha y'' \int_0^1 \Psi_1' y' \,dx + 4(\omega_1^{in})^2 \Psi_1 = -\Pi_1, \quad \Psi_2'' + \alpha y'' \int_0^1 \Psi_2' y' \,dx + 4(\omega_3^{in})^2 \Psi_2 = -\Pi_2, \tag{22}$$

$$\Psi_3'' + \alpha y'' \int_0^1 \Psi_3' y' \,dx + (\omega_1^{in} + \omega_3^{in})^2 \Psi_3 = -\Pi_3, \quad \Psi_4'' + \alpha y'' \int_0^1 \Psi_4' y' \,dx + (\omega_1^{in} - \omega_3^{in})^2 \Psi_4 = -\Pi_4, \tag{23}$$

$$\Psi_5'' + \alpha y'' \int_0^1 \Psi_5' y' \,dx = -\Pi_5, \quad \Psi_6'' + \alpha y'' \int_0^1 \Psi_6' y' \,dx = -\Pi_6, \tag{24}$$

$$\Psi_7'' + \alpha y'' \int_0^1 \Psi_7' y' \,dx + 4(\omega_3^{out})^2 = -\Pi_7, \quad \Psi_8'' + \alpha y'' \int_0^1 \Psi_8' y' \,dx = -\Pi_8, \tag{25}$$

$$\Psi_9'' + (\omega_1^{in} + \omega_3^{out})^2 \Psi_9 = -\Pi_9, \quad \Psi_{10}'' + (\omega_3^{in} + \omega_3^{out})^2 \Psi_{10} = -\Pi_{10}, \tag{26}$$

$$\Psi_{11}'' + (\omega_1^{in} - \omega_3^{out})^2 \Psi_{11} = -\Pi_{11}, \quad \Psi_{12}'' + (\omega_3^{in} - \omega_3^{out})^2 \Psi_{12} = -\Pi_{12}, \tag{27}$$

with all of the functions satisfying the boundary conditions: $\Psi_i(x)|_{x=0,x=1}=0$. Substituting Eqs. (15), (16), (20) and (21) into the third-order equations (12) and (13), we can obtain

$$\begin{aligned}D_0^2v_3-v_3''-\alpha y''\int_0^1 y'v_3'\,\mathrm{d}x=&-\mathrm{i}\omega_1^{\mathrm{in}}(D_2A_1+2c_vA_1)\mathrm{e}^{\mathrm{i}\omega_1^{\mathrm{in}}T_0}\phi_1-\mathrm{i}\omega_1^{\mathrm{in}}(D_2A_3+2c_vA_3)\mathrm{e}^{\mathrm{i}\omega_3^{\mathrm{in}}T_0}\phi_3\\&+\chi_1(x)A_1^2\bar{A}_1\mathrm{e}^{\mathrm{i}\omega_1^{\mathrm{in}}T_0}+\chi_2(x)A_1A_3\bar{A}_3\mathrm{e}^{\mathrm{i}\omega_1^{\mathrm{in}}T_0}+\chi_3(x)A_3\bar{A}_1\bar{A}_1\mathrm{e}^{\mathrm{i}(\omega_3^{\mathrm{in}}-2\omega_1^{\mathrm{in}})T_0}\\&+\chi_4(x)A_3A_1\bar{A}_1\mathrm{e}^{\mathrm{i}\omega_3^{\mathrm{in}}T_0}+\chi_5(x)A_3^2\bar{A}_3\mathrm{e}^{\mathrm{i}\omega_3^{\mathrm{in}}T_0}+\chi_6(x)A_1^3\mathrm{e}^{3\mathrm{i}\omega_1^{\mathrm{in}}T_0}\\&+\chi_7(x)A_1B_3\bar{B}_3\mathrm{e}^{\mathrm{i}\omega_1^{\mathrm{in}}T_0}+\chi_8(x)A_3B_3\bar{B}_3\mathrm{e}^{\mathrm{i}\omega_3^{\mathrm{in}}T_0}+\chi_9(x)B_3^2\bar{A}_3\mathrm{e}^{\mathrm{i}(2\omega_3^{\mathrm{out}}-\omega_3^{\mathrm{in}})T_0}\\&+\frac{F}{2}\mathrm{e}^{\mathrm{i}\Omega T_0}+\mathrm{cc}+\mathrm{NST},\end{aligned}\tag{28}$$

$$\begin{aligned}D_0^2w_3-w_3''=&-\mathrm{i}\omega_3^{\mathrm{out}}(D_2B_3+2c_wB_3)\mathrm{e}^{\mathrm{i}\omega_3^{\mathrm{out}}T_0}\varphi_3+\chi_{10}(x)B_3^2\bar{B}_3\mathrm{e}^{\mathrm{i}\omega_3^{\mathrm{out}}T_0}+\chi_{11}(x)A_3B_3\bar{A}_3\mathrm{e}^{\mathrm{i}\omega_3^{\mathrm{out}}T_0}\\&+\chi_{12}(x)B_3\bar{A}_1A_1\mathrm{e}^{\mathrm{i}\omega_3^{\mathrm{out}}T_0}+\chi_{13}(x)\bar{A}_3^2B_3\mathrm{e}^{\mathrm{i}(\omega_3^{\mathrm{out}}-2\omega_3^{\mathrm{in}})T_0}+\mathrm{cc}+\mathrm{NST},\end{aligned}\tag{29}$$

where NST stands for the terms that do not produce secular effects, $\chi_i(x)$ $(i=1,\ldots,6)$ are defined in Ref. [20], and $\chi_i(x)$ $(i=7,\ldots,13)$ are defined in Appendix B.

Because we only focus on the three-to-one and one-to-one resonances and the primary resonance, the detuning parameters σ_1, σ_2 and σ_3 are introduced to describe the nearness of the internal and primary resonances, defined as

$$\omega_3^{\mathrm{in}}=3\omega_1^{\mathrm{in}}+\varepsilon^2\sigma_1,\quad \omega_3^{\mathrm{out}}=\omega_3^{\mathrm{in}}+\varepsilon^2\sigma_2\quad\text{and}\quad\Omega=\omega_1^{\mathrm{in}}+\varepsilon^2\sigma_3.\tag{30}$$

Because the homogeneous problems governing v_3 and w_3 admit non-trivial solutions, the corresponding non-homogeneous problem has a solution only if the solvability conditions are satisfied. In this case, the right-hand sides of Eqs. (28) and (29) need to be orthogonal to every solution of the adjoint problem [2]. Therefore, we can obtain the following solvability conditions:

$$2\mathrm{i}\omega_1^{\mathrm{in}}(A_1'+\mu_1A_1)=\Gamma_{11}A_1^2\bar{A}_1+\Gamma_{12}A_1A_3\bar{A}_3+\Gamma_{13}A_3\bar{A}_1^2\mathrm{e}^{\mathrm{i}\sigma_1T_2}+\Gamma_{14}A_1B_3\bar{B}_3+\frac{f_1}{2}\mathrm{e}^{\mathrm{i}\sigma_3T_2},\tag{31}$$

$$2\mathrm{i}\omega_3^{\mathrm{in}}(A_3'+\mu_2A_3)=\Gamma_{21}A_3A_1\bar{A}_1+\Gamma_{22}A_3^2\bar{A}_3+\Gamma_{23}A_1^3\mathrm{e}^{-\mathrm{i}\sigma_1T_2}+\Gamma_{24}A_3B_3\bar{B}_3+\Gamma_{25}B_3^2\bar{A}_3\mathrm{e}^{2\mathrm{i}\sigma_2T_2},\tag{32}$$

$$2\mathrm{i}\omega_3^{\mathrm{out}}(B_3'+\mu_3B_3)=\Gamma_{31}B_3^2\bar{B}_3+\Gamma_{32}A_3\bar{A}_3B_3+\Gamma_{33}A_1B_3\bar{A}_1+\Gamma_{34}A_2^2\bar{B}_3\mathrm{e}^{-2\mathrm{i}\sigma_2T_2},\tag{33}$$

where the coefficients are defined in Appendix C, and the prime indicates the derivative with respect to T_2. For the case of the primary resonance, we can introduce the following polar transformations:

$$A_j=\tfrac{1}{2}a_j\mathrm{e}^{\mathrm{i}\beta_j},\ j=1,3\quad\text{and}\quad B_3=\tfrac{1}{2}b_3\mathrm{e}^{\mathrm{i}\psi_3},\tag{34}$$

where a_j, β_j, b_3 and ψ_3 are the undetermined real functions of T_2, and can be determined by imposing the solvability conditions. Substituting Eq. (34) into Eqs. (31)–(33), and separating the real and imaginary parts, we can obtain the following polar form of the modulation equations:

$$8\omega_1^{\mathrm{in}}a_1'=-8\omega_1^{\mathrm{in}}\mu_1a_1+\Gamma_{13}a_1^2a_3\sin\gamma_1+4f_1\sin\gamma_2,\tag{35}$$

$$8\omega_3^{\mathrm{in}}a_3'=-8\omega_3^{\mathrm{in}}\mu_2a_3-\Gamma_{23}a_1^3\sin\gamma_1+\Gamma_{25}b_2^3a_3\sin\gamma_3,\tag{36}$$

$$8\omega_3^{\mathrm{out}}b_3'=-8\omega_3^{\mathrm{out}}\mu_3b_3-\Gamma_{34}a_3^2b_3\sin\gamma_3,\tag{37}$$

$$8\omega_1^{\mathrm{in}}a_1\beta_1'=-\Gamma_{11}a_1^3-\Gamma_{12}a_1a_3^2-\Gamma_{13}a_1^2a_3\cos\gamma_1-\Gamma_{14}a_1b_3^2-4f_1\cos\gamma_2,\tag{38}$$

$$8\omega_3^{\mathrm{in}}a_3\beta_3'=-\Gamma_{21}a_1^2a_3-\Gamma_{22}a_3^3-\Gamma_{23}a_1^3\cos\gamma_1-\Gamma_{24}a_3b_3^2-\Gamma_{25}a_3b_3^2\cos\gamma_3,\tag{39}$$

$$8\omega_3^{\mathrm{out}}b_3\psi_3'=-\Gamma_{31}b_3^3-\Gamma_{32}b_3a_3^2-\Gamma_{33}b_3a_1^2-\Gamma_{34}b_3a_3^2\cos\gamma_3,\tag{40}$$

where $\gamma_1 = \beta_3 - 3\beta_1 + \sigma_1 T_2$, $\gamma_2 = \sigma_3 T_2 - \beta_1$, $\gamma_3 = 2(\psi_3 - \beta_3) + 2\sigma_2 T_2$. Therefore, we can obtain the following second-order expansion of the displacements for the case of the primary resonance of the first symmetric mode:

$$\begin{aligned} v(x,t) = {} & \varepsilon a_1 \cos(\Omega t - \gamma_2)\phi_1 + \varepsilon a_3 \cos(3\Omega t + \gamma_1 - 3\gamma_2)\phi_3 + \tfrac{1}{2}\varepsilon^2\{a_1^2[\cos 2(\Omega t - 2\gamma_2)\Psi_1 + \Psi_5] \\ & + a_3^2[\cos 2(3\Omega t + \gamma_1 - 3\gamma_2)\Psi_2 + \Psi_6] + b_3^2[\cos(6\Omega t + 2\gamma_1 - 6\gamma_2 + \gamma_3)\Psi_7 + \Psi_8] \\ & + a_1 a_3[\cos(4\Omega t + \gamma_1 - 4\gamma_2)\Psi_3 + \cos(2\Omega t + \gamma_1 - 2\gamma_2)\Psi_4]\} + \cdots, \end{aligned} \tag{41}$$

$$\begin{aligned} w(x,t) = {} & \varepsilon b_3 \cos(3\Omega t + \gamma_1 - 3\gamma_2 + 0.5\gamma_3)\varphi_3 + \tfrac{1}{2}\varepsilon^2\{a_1 b_3[\cos(4\Omega t + \gamma_1 - 4\gamma_2 + 0.5\gamma_3)\Psi_9 \\ & + \cos(2\Omega t + \gamma_1 - 2\gamma_2 + 0.5\gamma_3)\Psi_{11}] + a_3 b_3[\cos(6\Omega t + 2\gamma_1 - 6\gamma_2 + 0.5\gamma_3)\Psi_{10} \\ & + \cos(0.5\gamma_3)\Psi_{12}]\} + \cdots. \end{aligned} \tag{42}$$

4. Numerical results and discussions

This section contains details of the numerical solutions of the modulation equations for the chosen external and multiple internal resonances combination. In our calculations, to represent the conditions currently found in civil engineering, we choose the following non-dimensional parameter values: $\alpha = 198.5$ and $f = 0.042$, with the associated value of the Irvine parameter, $\lambda^2 = 22.563$. For this cable, $\omega_1^{\text{in}} = 5.2389$, $\omega_3^{\text{in}} = 15.7334$ and $\omega_3^{\text{out}} = 5\pi$. Clearly, the three-to-one internal resonance between the third and the first symmetric modes is nearly perfectly tuned ($\sigma_1 = 0.016$). It should be pointed out that the one-to-one internal resonance between the first symmetric and the first anti-symmetric in-plane mode and the two-to-one internal resonance between the first symmetric in-plane mode and the first symmetric out-of-plane mode can be activated in this case. However, these internal resonances have been investigated in previous studies [3,4,10]. Furthermore, the main objective of this study is to investigate the three-to-three-to-one internal resonances of the suspended cable. Therefore, these internal resonance are not considered in this study. Moreover, the corresponding second-order shape functions Ψ_i are shown in Fig. 2. It can be observed from Fig. 2 that the second-order functions exhibit, as expected, a symmetric character. Also we consider the fixed damping coefficients: $\mu_1 = 0.003$, $\mu_2 = 0.001$ and $\mu_3 = 0.001$.

The equilibrium solution of the modulation equations corresponds to the periodic motion of the cable, and it can be determined by setting $a_i' = \gamma_1' = \gamma_2' = b_3' = \psi_3' = 0$ ($i = 1, 3$) in the modulation equations and solving the nonlinear system by the Newton–Raphson method. To determine the stability of the equilibrium solution, we firstly introduce the following transformation:

$$A_1 = \tfrac{1}{2}(p_1 - \mathrm{i}q_1)\mathrm{e}^{\mathrm{i}\sigma_3 T_2}, \quad A_3 = \tfrac{1}{2}(p_2 - \mathrm{i}q_2)\mathrm{e}^{\mathrm{i}(3\sigma_3 - \sigma_1)T_2} \quad \text{and} \quad B_3 = \tfrac{1}{2}(p_3 - \mathrm{i}q_3)\mathrm{e}^{\mathrm{i}(3\sigma_3 - \sigma_1 - \sigma_2)T_2} \tag{43}$$

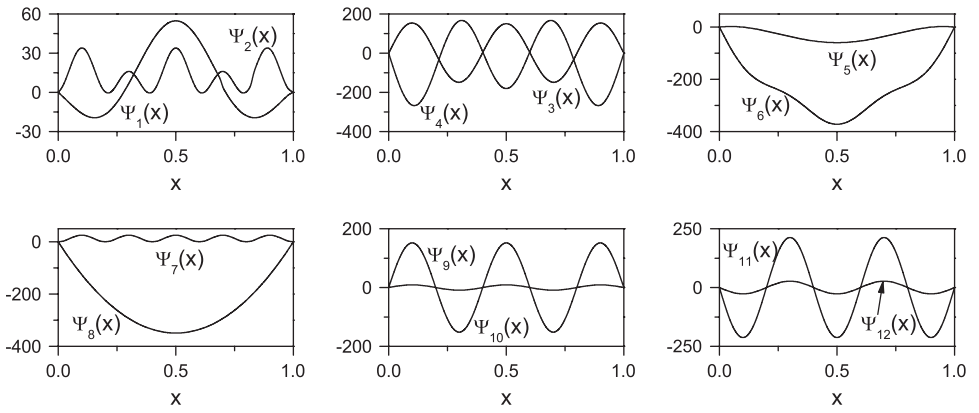

Fig. 2. The second-order shape functions $\Psi_i(x)$ when $\lambda^2 = 22.563$.

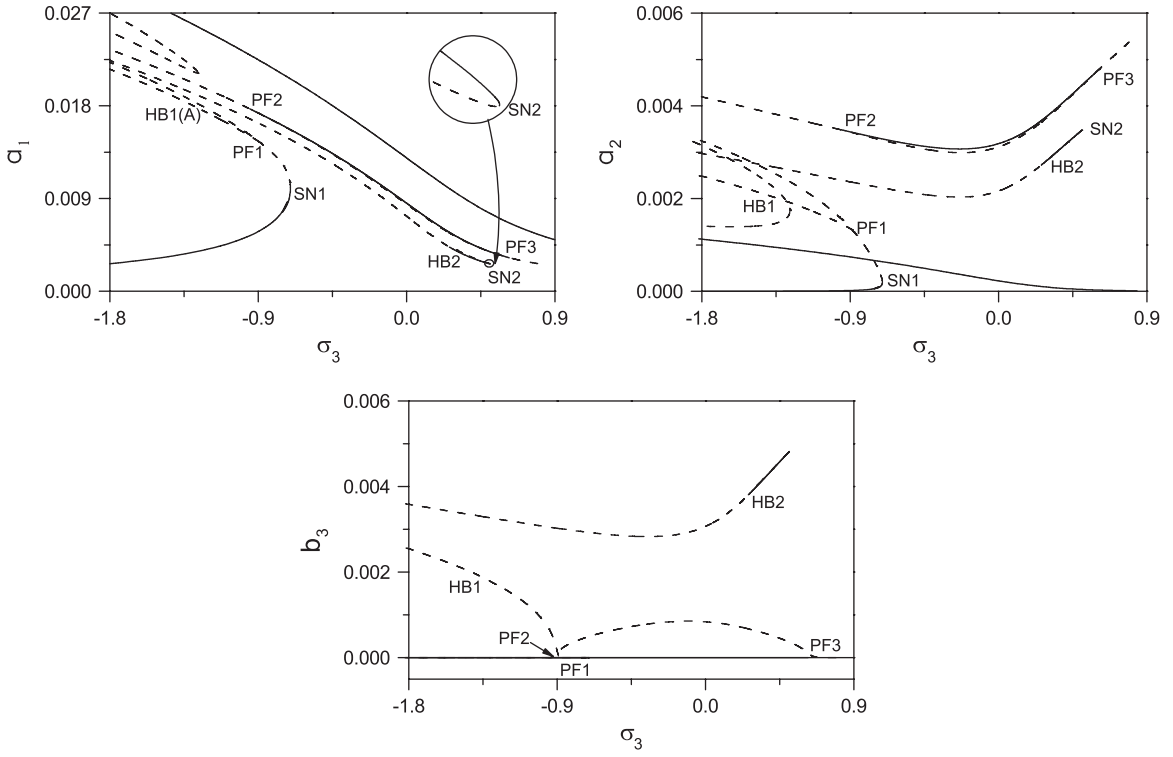

Fig. 3. Frequency–response curves of the cable with $f_1 = 0.005$ when $\Omega \approx \omega_1^{\text{in}}$.

to obtain the Cartesian form of the modulation equations. Then the stability of the solution is ascertained by examining the eigenvalues of the *Jacobian matrix*. After one solution is determined, the continuation method [25] can be used to trace the solution branch.

Fig. 3 illustrates the amplitudes of the first and third symmetric in-plane mode and the third symmetric out-of-plane mode of the taut cable as functions of the detuning parameter σ_3 in the neighborhood of the primary resonance of the first symmetric in-plane mode with $f_1 = 0.005$, where the solid and dashed lines indicate the stable and unstable solution, respectively, and SN, PF and HB represent the saddle-node, pitchfork and Hopf bifurcation points, respectively. As expected, the results shown in Fig. 3 exhibit a softening behavior for the frequency–response curves of the first symmetric in-plane mode. Also, the pure in-plane motion solution branches, $a_1 \neq 0$, $a_3 \neq 0$ and $b_3 = 0$, are found. Globally, these branches are similar to the ones calculated by Zhao and Wang [20]. However, due to the presence of the third symmetric out-of-plane mode in this case, the frequency–response curves of the in-plane modes reveal some difference.

As the detuning parameter σ_3 decreases from -0.702 at SN1, the amplitude of the unstable in-plane solution increases. When σ_3 is decreased beyond -0.907, the non-planar solution branch emerges as a result of a pitchfork bifurcation at PF1, resulting in reduction of the amplitudes of the in-plane solutions with respect to the one of the pure in-plane solutions. Following this non-planar solution branch, the real part of one pair of complex conjugate eigenvalues of *Jacobian matrix* decreases as σ_3 decreases, as shown in Fig. 4a, and the unstable solution undergoes a Hopf bifurcation at HB1 ($\sigma_3 \approx -1.329$), with the eigenvalues crossing the imaginary axis transversely (see Fig. 4a), resulting in a periodic solution with period $2\pi/|\beta|$, where β is the purely imaginary eigenvalue. However, the unstable solution branch does not gain its stability at HB1 (Fig. 4a). To obtain the periodic solution of the modulation equations, which corresponds to the quasi-periodic motion of the cable, the shooting method [25] is applied to solve the Cartesian form of the modulation equations, and the periodic solution's stability can be ascertained by the Floquet theory [25]. The periodic solution branches originating from HB1 are shown in Fig. 4b, where the amplitudes indicate the maximum and minimum values of p_1, which occur on the limit cycle, and the open circles denote the unstable periodic solutions. It can be observed from Fig. 4b that the periodic solution starting from HB1 is unstable.

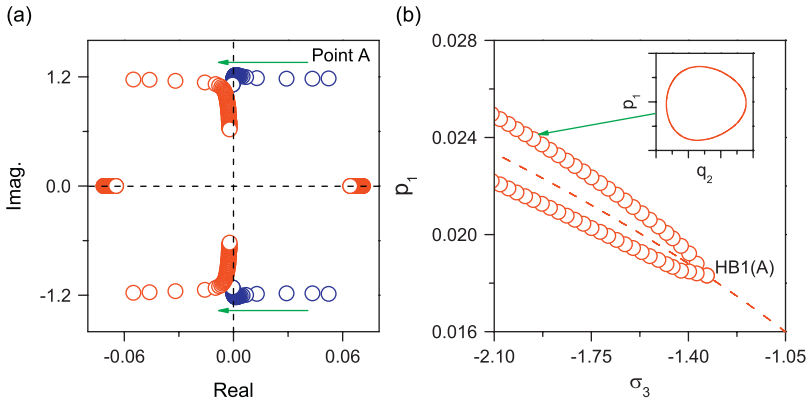

Fig. 4. Eigenvalues of the Jacobian matrix (a) and the periodic solutions branches of the modulation equations (b) when $\sigma_3 \approx -1.329$.

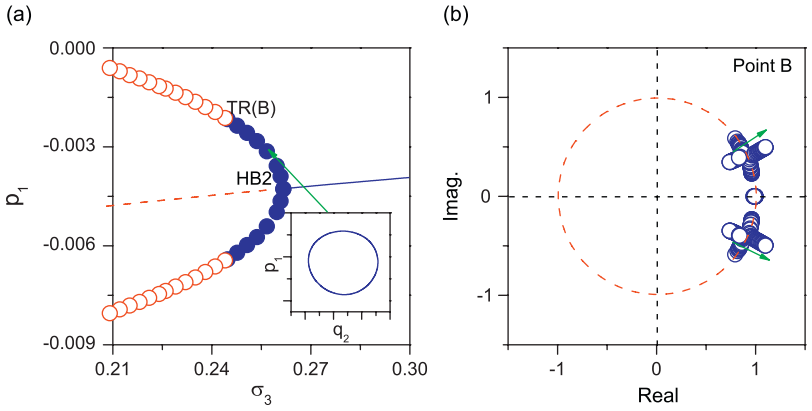

Fig. 5. The periodic solution branches of the modulation equations (a) and the corresponding Floquet multipliers in the complex plane (b) when $\sigma_3 \approx 0.246$.

Referring to Fig. 3, when $\sigma_3 < 0.791$, the modulation equations have another in-plane motion solution. This unstable solution gains its stability via a subcritical pitchfork bifurcation at PK3, and loses its stability when another subcritical pitchfork bifurcation occurs at PK2. As the result of these bifurcations, unstable non-planar solutions can be observed between PK2 and PK3. Due to the one-to-one internal resonance, the non-planar solution branches, $a_1 \neq 0$, $a_3 \neq 0$ and $b_3 \neq 0$, can also be activated. This fact is clearly illustrated in Fig. 3. As σ_3 increases from a small value, the unstable non-planar solution gains stability via a Hopf bifurcation at HB2 ($\sigma_3 \approx 0.306$), and then the solution experiences a saddle-node bifurcation at SN2 ($\sigma_3 \approx 0.501$), resulting in a jump to the in-plane solution.

On continuing the periodic solutions emerging from HB2 in Fig. 3, Fig. 5a shows the periodic solutions of the modulation equations as σ_3 varies, where the filled circles denote the stable periodic solutions and TR denotes the torus bifurcation point. It can observed from Fig. 5a that the Hopf bifurcation (HB2) is supercritical due to the fact that the periodic solution starting from HB2 is stable. Starting from $\sigma_3 = 0.306$, the limit cycle grows from a zero amplitude to some finite size as σ_3 increases. The period-1 (P-1) solution is stable over the detuning interval $\sigma_3 \in (0.245, 0.306)$, and loses its stability when a bifurcation occurs at Point B. To determine the bifurcation type, Fig. 5b shows the Floquet multipliers of the periodic solution as the detuning parameter σ_3 decreases from 0.306. It is interesting to note that one complex conjugate pair of Floquet multipliers crosses the unit circle away from the real axis. This indicates the occurrence of the torus bifurcation. Therefore, the non-planar solution of the modulation equations should become quasi-periodic in this case. To demonstrate the existence of a quasi-periodic solution, the modulation equations are numerically integrated by employing the Runge–Kutta method. Fig. 6a shows the steady-state time history of the

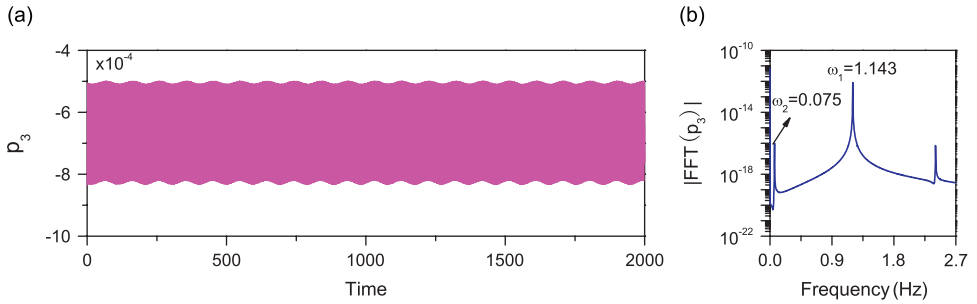

Fig. 6. The quasi-periodic solution of the modulation equation with $\sigma_3 = 0.244$. (a) The time history; (b) the power spectrum.

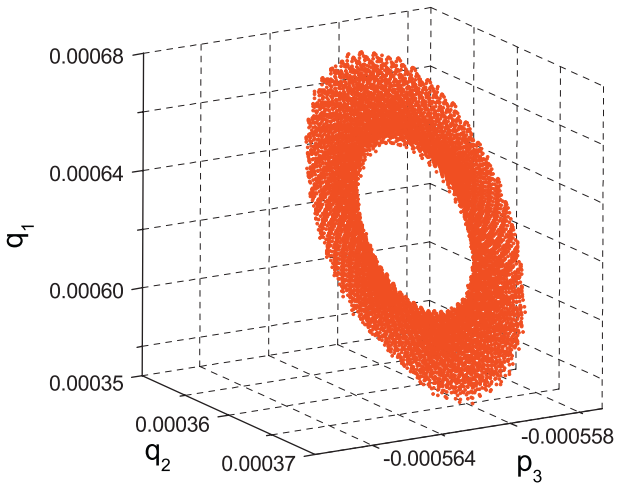

Fig. 7. The Poincaré section of the quasi-periodic solution.

modulation equations at $\sigma_3 = 0.244$. It is observed that the amplitude of time history varies with a particular period. In order to identify the nonlinear frequency components in this time history, the time history is analyzed by the fast Fourier transform (FFT). Fig. 6b shows the power spectrum of the time history of the modulation equations. As shown in Fig. 6b, two fundamental frequency components ($\omega_1 = 1.143, \omega_2 = 0.075$) are found. Both of these indicate the quasi-periodic character of the solution. Fig. 7 shows the Poincaré section of this quasi-periodic solution in a 3-D space. This Poincaré section shows a closed curve in the 3-D space, indicating the quasi-periodic character of the solution again. Clearly, the 2-D projection of the Poincaré section is very difficult to clarify the topology of the quasi-periodic attractor. By reducing the detuning parameterσ_3 further, the quasi-periodic solution undergoes destruction of the torus, resulting in chaos, and a representative chaotic attractor is shown in Fig. 8. It is shown that the trajectories tend to fill up a specific section of the phase plane (Fig. 8a); the spectrum consists of a distributed spectrum (Fig. 8b), confirming the chaotic nature of this attractor. However, the stable chaotic attractor only exists in a very narrow region, and as σ_3 decreases further, it encounters a boundary crisis. This crisis, due to the attractor colliding with an unstable orbit within its basin of attraction, gives rise to a stable in-plane equilibrium solution, as shown in Fig. 9.

In order to investigate the effects of excitation amplitudes on the frequency–response curves of the taut cable, we present the results for relatively high amplitudes, i.e., $f_1 = 0.0095$. The frequency–response curves of the cable for the case of the primary resonance of the first symmetric mode with $f_1 = 0.0095$ are shown in Fig. 10. As the excitation amplitude increases, the amplitude of nonlinear response of the taut cable increases, resulting in multimode interactions and strengthening of nonlinearity . And a wider region of stable

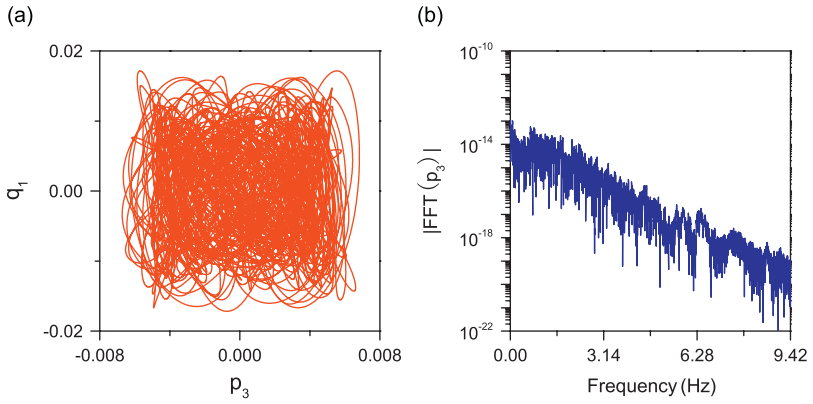

Fig. 8. The chaotic solution of the modulation equation with $\sigma_3 = 0.243$. (a) The phase plane; (b) the power spectrum.

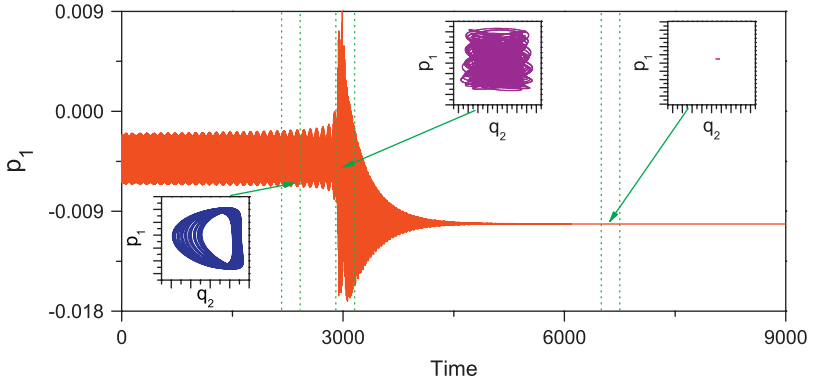

Fig. 9. The time history of the modulation equations at $\sigma_3 = 0.2425$ after a crisis occurs.

non-planar solution is observed. However, compared with Fig. 3, the frequency–response curves in Fig. 10 do not exhibit any significant difference, even though the excitation amplitude is increased nearly by 100%.

Fig. 11 shows the amplitude of the equilibrium solution as functions of the excitation amplitude f_1 for the negative detuning $\sigma_3 = -1.5$. There are two pitchfork bifurcation in the curves, and two non-planar solution branches emerge from these two bifurcations. Decreasing from $f_1 \approx 0.106$ at PK1, a newborn non-planar solution is observed, and gains its stability via a saddle-node bifurcation at SN3, then loses its stability when a Hopf bifurcation occurs at HB1. Moreover, starting from $f_1 \approx 0.138$ at PK2, a stable non-planar solution branch is also found. As is clear from the force–response curves in Fig. 11, two Hopf bifurcations at HB2 and HB3 can be noticed in the in-planar solution branch. These bifurcations also confirm the results obtained by Zhao and Wang [20].

5. Conclusions

In this paper, we investigated the nonlinear response of a shallow suspended cable with three-to-one and one-to-one internal resonances for the case of the primary resonance of the first symmetric in-plane mode. The method of multiple scales is used to obtain the modulation equations governing the amplitude and phase of the nonlinear response.

The Newton–Raphson method and a continuation method were applied to determine the frequency–response and force–response curves. These curves showed that the one-to-one internal resonance may result in a non-planar solution via a pitchfork bifurcation. Also, an isolated non-planar solution branch is observed in the frequency–response curves, and the stable non-planar solution may encounter a Hopf bifurcation.

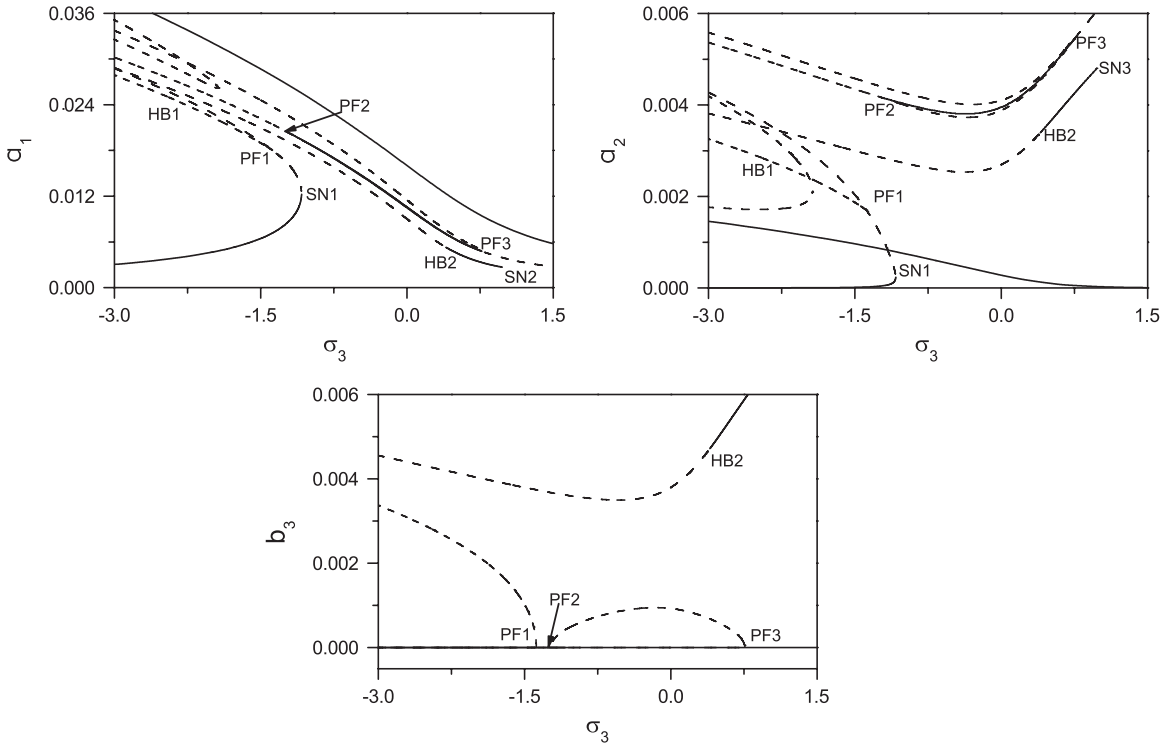

Fig. 10. Frequency–response curves of the cable with $f_1 = 0.0095$.

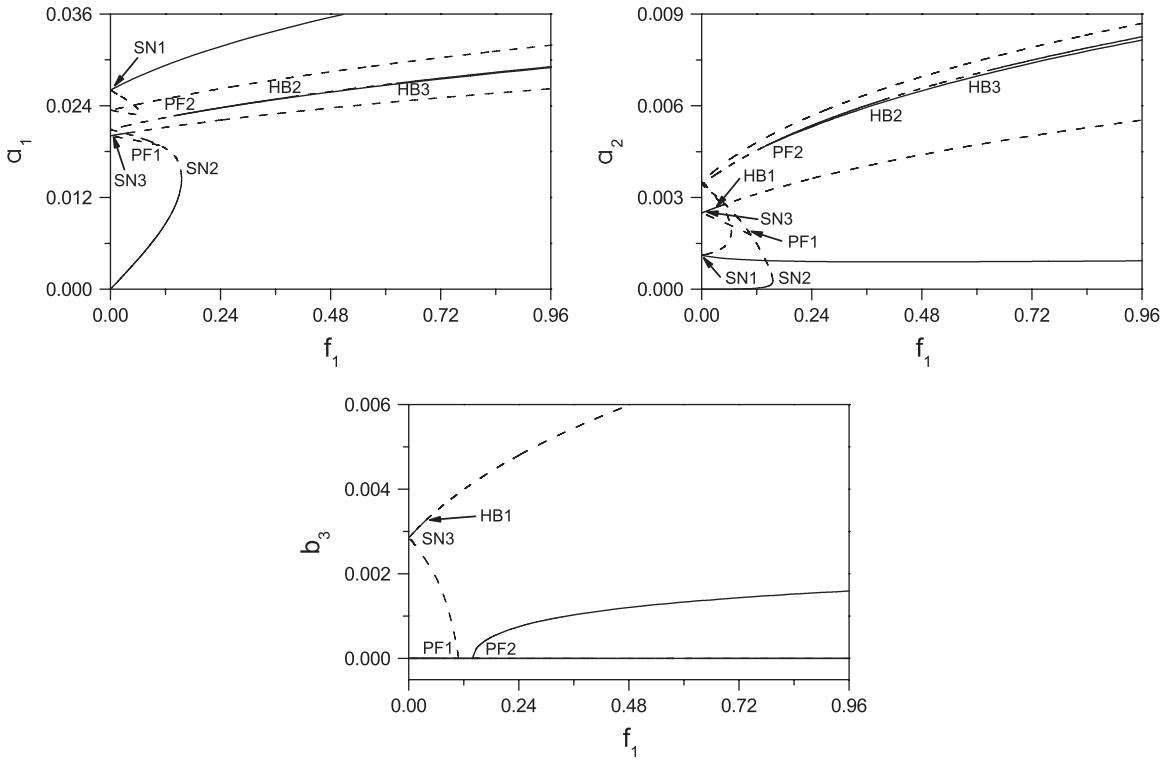

Fig. 11. Force–response curves of the cable with $\sigma_3 = -1.5$.

The shooting method and numerical simulations were used to investigate the dynamic solution of the modulation equations. The results showed that the chaotic attractor may appear in the phase plane as a consequence of the quasi-periodic solution undergoing the destruction of the torus. Then this attractor was destroyed through a crisis, resulting in an in-plane solution.

Acknowledgments

The study was supported by National Science Foundation of China under Grant nos. 10502020 and 10772065.

Appendix A

The symmetric in-plane modes are given by

$$\phi_i(x) = c_i[1 - \tan(\tfrac{1}{2}\omega_i^{\text{in}})\sin\omega_i^{\text{in}}x - \cos\omega_i^{\text{in}}x], \quad i = 1, 2, 3, \ldots, \tag{A.1}$$

where c_i are chosen so that the modes satisfy the orthonormality condition. And the frequencies are determined by

$$\frac{1}{2}\omega_i^{\text{in}} - \tan\left(\frac{\omega_i^{\text{in}}}{2}\right) - \frac{1}{2\lambda^2}(\omega_i^{\text{in}})^3 = 0, \tag{A.2}$$

where $\lambda^2 = EA/mgl(8b/l)^3$. The symmetric out-of-plane modes and frequencies are given by

$$\varphi_i(x) = \sqrt{2}\sin(2i-1)\pi x, \quad \omega_i^{\text{out}} = (2i-1)\pi, \ \ i = 1, 2, 3, \ldots\ . \tag{A.3}$$

Appendix B

The expressions of $\chi_i(x)$ $(i = 7, \ldots, 13)$ are

$$\chi_7(x) = \alpha\phi_1''\int_0^1 (2\Psi_8'y' + \varphi_3'\varphi_3')\,\mathrm{d}x + \alpha y''\int_0^1 (2\phi_1'\Psi_8' + \Psi_9'\varphi_3' + \Psi_{11}'\varphi_3')\,\mathrm{d}x + 2\alpha\Psi_8''\int_0^1 \phi_1'y'\,\mathrm{d}x, \tag{B.1}$$

$$\chi_8(x) = \alpha\phi_3''\int_0^1 (2\Psi_8'y' + \varphi_3'\varphi_3')\,\mathrm{d}x + \alpha y''\int_0^1 (2\phi_3'\Psi_8' + \Psi_{10}'\varphi_3' + \Psi_{12}'\varphi_3')\,\mathrm{d}x + 2\alpha\Psi_8''\int_0^1 \phi_1'y'\,\mathrm{d}x, \tag{B.2}$$

$$\chi_9(x) = \alpha\phi_3''\int_0^1 \Psi_7'y'\,\mathrm{d}x + \alpha y''\int_0^1 (\phi_3'\Psi_7' + \Psi_{12}'\varphi_3')\,\mathrm{d}x + \alpha\Psi_7''\int_0^1 \phi_3'y'\,\mathrm{d}x, \tag{B.3}$$

$$\chi_{10}(x) = \alpha\varphi_3''\int_0^1 \left(\Psi_7'y' + 2\Psi_8'y' + \frac{3}{2}\varphi_3'\varphi_3'\right)\mathrm{d}x, \tag{B.4}$$

$$\chi_{11}(x) = \alpha\varphi_3''\int_0^1 (2\Psi_6'y' + \phi_3'\phi_3')\,\mathrm{d}x + \alpha(\Psi_{10}'' + \Psi_{12}'')\int_0^1 y'\phi_3'\,\mathrm{d}x, \tag{B.5}$$

$$\chi_{12}(x) = \alpha\varphi_3''\int_0^1 (2\Psi_5'y' + \phi_1'\phi_1')\,\mathrm{d}x + \alpha(\Psi_9'' + \Psi_{11}'')\int_0^1 y'\phi_1'\,\mathrm{d}x, \tag{B.6}$$

$$\chi_{13}(x) = \alpha\varphi_3''\int_0^1 \left(\frac{1}{2}\phi_3'\phi_3' + \Psi_2'y'\right)\mathrm{d}x + \alpha\Psi_{12}''\int_0^1 y'\phi_3'\,\mathrm{d}x. \tag{B.7}$$

Appendix C

The coefficients of the modulation equations are

$$\mu_1 = \int_0^1 c_v\phi_1^2\,\mathrm{d}x, \quad \mu_2 = \int_0^1 c_v\phi_3^2\,\mathrm{d}x, \quad \mu_3 = \int_0^1 c_w\varphi_3^2\,\mathrm{d}x, \quad f_1 = \int_0^1 F\phi_1\,\mathrm{d}x,$$
$$\Gamma_{11} = \int_0^1 \chi_1\phi_1\,\mathrm{d}x, \quad \Gamma_{12} = \int_0^1 \chi_2\phi_1\,\mathrm{d}x, \quad \Gamma_{13} = \int_0^1 \chi_3\phi_1\,\mathrm{d}x, \quad \Gamma_{14} = \int_0^1 \chi_7\phi_1\,\mathrm{d}x,$$
$$\Gamma_{21} = \int_0^1 \chi_4\phi_3\,\mathrm{d}x, \quad \Gamma_{22} = \int_0^1 \chi_5\phi_3\,\mathrm{d}x, \quad \Gamma_{23} = \int_0^1 \chi_6\phi_3\,\mathrm{d}x,$$
$$\Gamma_{24} = \int_0^1 \chi_8\phi_3\,\mathrm{d}x, \quad \Gamma_{25} = \int_0^1 \chi_9\phi_3\,\mathrm{d}x,$$
$$\Gamma_{31} = \int_0^1 \chi_{10}\varphi_3\,\mathrm{d}x, \quad \Gamma_{32} = \int_0^1 \chi_{11}\varphi_3\,\mathrm{d}x, \quad \Gamma_{33} = \int_0^1 \chi_{12}\varphi_3\,\mathrm{d}x, \quad \Gamma_{34} = \int_0^1 \chi_{13}\varphi_3\,\mathrm{d}x. \tag{C.1}$$

References

[1] G. Rega, Nonlinear vibrations of suspended cables. Part I: modeling and analysis, Part II: deterministic phenomena, *Applied Mechanics Reviews* 57 (2004) 443–478 479–514.

[2] A.H. Nayfeh, *Non-linear Interactions*, Wiley-Interscience, New York, 2000.

[3] M. Pakdemirli, S.A. Nayfeh, A.H. Nayfeh, Analysis of one-to-one autoparametric resonances in cables: discretization versus direct treatment, *Nonlinear Dynamics* 8 (1995) 65–83.

[4] Y.Y. Zhao, L.H. Wang, D.L. Chen, L.Z. Jiang, Nonlinear dynamic analysis of the two-dimensional simplified model of an elastic cable, *Journal of Sound and Vibration* 255 (2002) 43–59.

[5] G.V. Rao, R.N. Iyengar, Internal resonance and non-linear response of a cable under periodic excitation, *Journal of Sound and Vibration* 149 (1991) 25–41.

[6] N.C. Perkins, Modal interactions in the non-linear response of elastic cables under parametric/external excitation, *International Journal of Non-linear Mechanics* 27 (1992) 233–250.

[7] C.L. Lee, N.C. Perkins, Non-linear oscillations of suspended cables containing a two-to-one internal resonance, *Nonlinear Dynamics* 3 (1993) 465–490.

[8] N. Srinil, G. Rega, S. Chucheepsakul, Two-to-one resonant multi-modal dynamics of horizontal/inclined cables. Part I: theoretical formulation and model validation, *Nonlinear Dynamics* 48 (2006) 231–252.

[9] N. Srinil, G. Rega, Two-to-one resonant multi-modal dynamics of horizontal/inclined cables. Part II: internal resonance activation, reduced-order models and nonlinear normal modes, *Nonlinear Dynamics* 48 (2006) 253–274.

[10] V. Gattulli, L. Martinelli, F. Perotti, F. Vestroni, Nonlinear oscillations of cables under harmonic loading using analytical and finite element models, *Computer Methods in Applied Mechanics and Engineering* 193 (2004) 69–85.

[11] C.L. Lee, N.C. Perkins, Three-dimensional oscillations of suspended cables involving simultaneous internal resonances, *Nonlinear Dynamics* 8 (1995) 45–63.

[12] F. Benedettini, G. Rega, R. Alaggio, Nonlinear oscillations of a four-degree-of-freedom model of a suspended cable under multiple internal resonance conditions, *Journal of Sound and Vibration* 182 (1995) 775–798.

[13] G. Rega, W. Lacarbonara, A.H. Nayfeh, C.-M. Chin, Multiple resonances in suspended cables: direct versus reduced-order models, *International Journal of Non-linear Mechanics* 34 (1999) 901–924.

[14] A.H. Nayfeh, H.N. Arafat, C.-M. Chin, W. Lacarbonara, Multimode interactions in suspended cables, *Journal of Vibration and Control* 8 (2002) 337–387.

[15] J.A. Main, N.P. Jones, Free vibrations of taut cable with attached damper. I: linear viscous damper, *Journal of Engineering Mechanics, ASCE* 128 (2002) 1062–1071.

[16] E.A. Johnson, G.A. Baker, B.F. Spencer Jr., Y. Fujino, Semiactive damping of stay cables, *Journal of Engineering Mechanics, ASCE* 133 (2007) 1–11.

[17] T. Susumpow, Y. Fujino, Active control of multimodal cable vibrations by axial support motion, *Journal of Engineering Mechanics, ASCE* 121 (1995) 964–972.

[18] Y.L. Xu, S. Zhan, J.M. Ko, Z. Yu, Experimental study of vibration mitigation of bridge stay cables, *Journal of Structural Engineering, ASCE* 125 (1999) 977–986.

[19] W. Lacarbonara, G. Rega, Resonate nonlinear normal modes. Part II: activation/orthogonality conditions for shallow structural systems, *International Journal of Non-linear Mechanics* 38 (2003) 873–887.

[20] Y. Zhao, L. Wang, On the symmetric modal interaction of the suspended cable: three-to-one internal resonance, *Journal of Sound and Vibration* 294 (2006) 1073–1093.

[21] L. Wang, Y. Zhao, Nonlinear interactions and chaotic dynamics of suspended cables with three-to-one internal resonances, *International Journal of Solids and Structures* 43 (2006) 7800–7819.
[22] L. Wang, Y. Zhao, Non-linear planar dynamics of suspended cables investigated by the continuation technique, *Engineering Structures* 29 (2007) 1135–1144.
[23] H.N. Arafat, A.H. Nayfeh, Non-linear responses of suspended cables to primary resonance excitations, *Journal of Sound and Vibration* 266 (2003) 325–354.
[24] A.H. Nayfeh, D.T. Mook, *Nonlinear Oscillations*, Wiley-Interscience, New York, 1997.
[25] A.H. Nayfeh, B. Balachandran, *Applied Nonlinear Dynamics*, Wiley-Interscience, New York, 1994.